CORA Cork Open Research Archive
Cartlann Taighde Oscailte Chorcaí

Title	A simulation and experimental study of electrochemical pH control at gold interdigitated electrode arrays
Authors	O'Sullivan, Benjamin;Patella, Bernardo;Daly, Robert;Seymour, Ian;Robinson, Caoimhe;Lovera, Pierre;Rohan, James F.;Inguanta, Rosalinda;O'Riordan, Alan
Publication date	2021-08-22
Original Citation	O'Sullivan, B., Patella, B., Daly, R., Seymour, I., Robinson, C., Lovera, P., Rohan, J., Inguanta, R. and O'Riordan, A. (2021) 'A simulation and experimental study of electrochemical pH control at gold interdigitated electrode arrays', Electrochimica Acta, 395, 139113 (9pp). doi: 10.1016/j.electacta.2021.139113
Type of publication	Article (peer-reviewed)
Link to publisher's version	10.1016/j.electacta.2021.139113
Rights	© 2021, Elsevier Ltd. All rights reserved. This manuscript version is made available under the CC BY-NC-ND 4.0 license. - https://creativecommons.org/licenses/by-nc-nd/4.0/
Download date	2026-10-13 17:03:20
Item downloaded from	https://hdl.handle.net/10468/11946

UCC
University College Cork, Ireland
Coláiste na hOllscoile Corcaigh

A Simulation and Experimental Study of Electrochemical pH Control at Gold Interdigitated Electrode Arrays

Benjamin O'Sullivan[a], Bernardo Patella[a,b], Robert Daly[a], Ian Seymour[a,c], Caoimhe Robinson[a], Pierre Lovera[a], James F. Rohan[c], Rosalinda Inguanta[b], Alan O'Riordan[a]

a Nanotechnology Group, Tyndall National Institute, University College Cork, Cork T12 R5CP, Ireland

b Laboratorio di Chimica Fisica Applicata, Dipartimento di Ingegneria, Università of Palermo, Viale delle Scienze, Palermo, Italy

c Electrochemical Materials and Energy Group, Tyndall National Institute, University College Cork, Cork T12 R5CP, Ireland

Corresponding Author: alan.oriordan@tyndall.ie

Abstract

In electroanalysis, solution pH is a critical parameter that often needs to be tailored and controlled for the detection of particular analytes. This is most commonly performed by the addition of chemicals, such as strong acids or bases. Electrochemical in-situ pH control offers the possibility for the local adjustment of pH at the point of detection, without the need for additional reagents. Finite element analysis (FEA) simulations have been performed on interdigitated electrodes, to guide experimental design in relation to both electroanalysis and in-situ control of solution pH. No previous model exists that describes the generation of protons at an interdigitated electrode arrays in solution with one comb acting as a protonator, and the other as the sensor. In this work, FEA models are developed to provide insight into the optimum conditions necessary for electrochemical pH control. The magnitude of applied galvanostatic current has a direct relation to the flux of protons generated and subsequent change in pH. Increasing the separation between the electrodes increases the time taken for protons to diffuse across the gap between the electrode combs. The final pH achieved after 1 second, at both protonator and sensor electrodes, was

shown to be largely uninfluenced by the solution's initial pH. The impact of buffer concentration was modelled and investigated. In practice, the pH at the electrode surface was probed by means of cyclic voltammetry, i.e., to identify the potential of the gold oxide reduction peak. A pH indicator, methyl red, was used to visualise the solution pH change at the electrodes, comparing well with the model's prediction. Finally, we show that in-situ pH controlled detection of mercury in water, using square wave stripping voltammetry, is almost identical to samples acidified to pH 3.5 using nitric acid.

Keywords

Finite element analysis simulation, tailored in-situ pH control, solid state sensors, Electroanalysis, Microband interdigitated electrode array.

1. Introduction

The pH of a solution is an important parameter in many biological and chemical reactions, as either a catalyst, or, where the protons are active as reactant or product. The detection of numerous analytes, including porphyrins [1], nitrates/nitrites [2, 3], chlorine [4], silver [5], and a range of biomarkers [6-8], requires the adjustment of pH from neutral to acidic conditions. The typical method of changing solution pH is the rudimentary addition of buffers or strong acids and bases. A number of issues can arise from this method including the purchase and use of additional chemicals, the added safety risk and finally the potential to act as a source of contamination. Controlling the pH by in-situ electrochemical methods allows the user to adjust the pH both temporally and spatially and perform electroanalysis with the same device, thereby eliminating the extra steps. Potentially important electrochemical pH control methods include

electrochemical redox reactions [9] and water electrolysis [10]. The latter is the splitting of water with an electrical current and used to reduce the solution pH by applying a positive potential to consume hydroxyl ions in a basic solution or produce protons in acidic conditions. Heavy metals are analytes of interest due to their toxicity to humans and the environment and require routine monitoring. Electrochemistry is one approach that enables remote analysis. Mercury for example, is readily detected by stripping voltammetry, has been researched extensively [11-14], and is used herein as an exemplar molecule to demonstrate the applicability of electrochemical pH control.

Finite element analysis (FEA) simulations have been used to provide valuable insight into a variety of electrochemical processes. Mass transport at electrode arrays has been modelled to determine inter-electrode spacing needed to achieve diffusional independence [15, 16]. The simulations directly informed the subsequent sensor design and fabrication. Similarly, the theoretical study of ionic transfer at liquid-liquid interfaces has guided the development of micro and nano-ITIES (interface between two immiscible electrolyte solutions) systems [17]. Adsorption processes at electrode surfaces have also been simulated, to assess reactions taking place at the electrode as the electrode itself is modified [18]. Wahl et al. demonstrated the use of simulations for iron detection at interdigitated microband electrodes(IDE) and the expected collection efficiency in generator-collector(GC) mode [19]. The spacing between the electrode combs is inversely proportional to the diffusional overlap and thus, at smaller inter-comb distances a greater degree of overlap is present.

The modelling of solution pH change and its effects have also been used to inform experimental design and compare to results. Read et al. [13] modelled the change in pH at concentric boron doped diamond ring electrodes. Protons were generated at the outer electrode and the decreased

local pH was monitored by use of an iridium oxide electrode. While elegant, this model did not account for a solution that contained buffering agents. Critelli et al. [20] have shown the effect of buffer reacting with generated protons and the impact on the rate of solution pH change. Proton flux, buffering effects and competing simultaneous chemical reactions were all investigated. While this model focused on the effects of probing the pH near the electrode surface, similar equations are applicable to models focused on directly changing the local pH. The combination of both models would allow the simulation of proton flux generated by a fixed current and the subsequent buffering effects to be taken into account.

In this work, FEA simulations were performed for proton generation by water electrolysis. This approach builds upon the works of Read and Critelli mentioned above by modelling the generation of protons at one comb of interdigitated electrodes and their buffered diffusion towards the other comb and the bulk solution. A galvanostatic current was applied at one comb, with the flux of protons proportional to the applied current. The importance of inter-electrode distance was investigated by modelling the proton generation at three different electrode separations. In response to these simulations, gold interdigitated microband arrays were designed and fabricated for the monitoring and control of solution pH. Solution buffer capacity was also investigated as it can affect the change in pH at the surface of the sensing electrodes. In our approach, the electrochemical gold oxide reduction peak was used as a probe to monitor local solution pH at the working electrodes; across a range of pH buffers. The change in solution pH by electrochemical control at an electrode array was also visualized optically by use of a pH indicator, methyl red. The region of colour change was then compared to simulated proton concentration profiles. Finally, mercury detection by anodic stripping analysis using both chemical and electrochemical pH control was demonstrated.

2. Experimental

2.1. Materials and electrode characterization

Nitric acid (35%), sodium chloride, ferrocene carboxylic acid (FcCOOH), phosphate buffer saline (PBS) tablets, mercury chloride, disodium phosphate and citric acid were purchased from Sigma Aldrich, Ireland and used as received. All solutions were prepared with DI water with resistivity of 18 MΩ cm^{-1}. A CHI 920 bi-potentiostat was used for the analytical measurements with the images captured on a Zeiss microscope equipped with a charge-coupled detector camera (CCD). All experiments were undertaken in a four electrode cell comprising of an on chip gold counter electrode and either an Ag/AgCl as external reference electrode or the on chip platinum pseudo reference electrode. The interdigitated working electrodes were electrochemically characterized by cyclic voltammetry using 1 mM FcCOOH in 10 mM PBS pH 7.4 solution. The potential was cycled between -0.15 V and 0.45 V vs. an on chip platinum pseudo-reference electrode with a scan rate of 100 mV/s. Sensing electrodes of 1 μm width with a 2 μm gap to the protonators typically exhibited a plateau current of 10 nA in non-GC mode, and 28 nA in GC mode analysis.

2.2. Electrode fabrication

Silicon chip sensor devices, consisting of an SD pinout, interdigitated gold microband electrode arrays, a gold counter electrode and a platinum pseudo reference electrode, were fabricated as described previously [19, 21]; see Fig. S1A. In brief, interdigitated gold microbands were

patterned in resist by photolithography followed by metal evaporation (Ti/Au 5/50 nm) and standard lift-off. Similarly, photolithography, metal evaporation (Ti/Au 10/90), and lift-off procedures were then employed to overlay electrical interconnection tracks including peripheral probe pads. Macroscale gold and platinum counter and pseudo-reference electrodes, respectively, were also deposited during this process. The counter and reference electrodes were maintained 830 and 1040 μm, respectively, from the working electrode. Finally, a silicon nitride passivation layer (500 nm thick) was deposited to passivate the entire chip and windows selectively opened with a dry etch to allow exclusive contact between the working, reference and counter electrodes with the solution of interest.

2.3. Gold oxide reduction peak

The effect of the solution pH on gold oxide reduction peak was studied. Gold oxide was formed and then reduced by cyclic voltammetry over a potential range of -0.15 V to 1.2 V on a gold working electrode array at 100 mV/s. The solution pH was varied chemically over a range of pH 3 to 8 by preparing a series of buffer solutions prepared by mixing different concentrations of citric acid and disodium phosphate. For electrochemical pH control, a series of potentials high enough to induce water electrolysis (1.3 V to 1.70 V) was applied to the protonator electrode array during the CV in PBS solution.

2.4. pH change visualisation

An artificial drinking water solution (ADW) containing the pH indicator, methyl red, was used to visually observe the change in pH. ADW was made up by dissolving 1 g of sodium bicarbonate, 0.0654 g of magnesium sulfate (Sigma Aldrich, 99.5% anhydrous), 0.3414 g calcium sulfate dihydrate (Honeywell, 99%), 0.007 g potassium phosphate dibasic (Fluka, 98%), 0.003 g potassium phosphate monobasic (Sigma Aldrich, 99%) and 0.01 g sodium nitrate (Sigma Aldrich, 99%) in 10 litres of deionized water. 50 mg of methyl red was dissolved in 25 ml of ethanol. This solution was then made up to 250 mL with ADW solution. A portable CHI 1222c potentiostat was used for visualization experiments. A current of 500 nA was applied at the protonator. The images were captured on a Zeiss microscope equipped with a charge-coupled detector camera. Image analysis software, ImageJ, was employed to estimate the diameter of the region of colour change. Images were split in RGB stacks, and the change in colour intensity across the figure was used to determine the diameter of the region of colour change.

2.5. Electrochemical Detection of Mercury

To demonstrate pH controlled metal detection, a 75 ppb (373 nM) mercury standard was prepared in DI water by dilution of a 1 g/ L stock solution in 10 mM NaCl. This solution was acidified using nitric acid for chemical pH control experiments. Interdigitated electrodes, with 2µm gaps, were used to detect mercury with both electrochemically acidified and chemically acidified solutions. Mercury analysis was performed by square wave anodic stripping voltammetry using the on-chip counter electrode and an external Ag/AgCl reference electrode. Prior to the stripping experiments, the chips were washed with pure isopropanol and deionized (DI) water in order to remove any contaminants from the electrode surface. Mercury was

deposited onto the microband electrodes by applying a fixed potential of -0.5 V for 120 s. The mercury was stripped by SWV with a potential window of -0.6 V to 0.8 V. Stripping peak current increased in more acidic media and reached a maximum at pH 3.5, which was then selected for mercury detection. A corresponding peak maximum was found for electrochemical pH control using an applied protonator voltage of 1.74 V.

3. Theory

GC electrode array devices comprised of two combs of interdigitated electrodes were employed for in-situ pH control in this work. A comb, in this regard, refers to one half of an interdigitated electrode array. The interdigitated electrodes were spaced 2 μm apart. By imposing an appropriate potential at one ("protonator") comb of electrodes, a pH change occurs in the local environment that tailors the pH at the other ("sensor") comb. The sensor comb may then be used to perform sensing in conditions that differ from the bulk solution. Fig. S2A shows a schematic of the in-situ pH control concept. In our approach, hydrolysis of water is employed to produce protons at the protonator electrode, which then diffuse to and lower the pH in the region of the sensor electrode; compared to the bulk solution.[13] The pH may be tailored to the required value by judicious control of the applied current density.[22] In acidic conditions, the pH can be changed through the water splitting reactions of equations 1-2:[23]

$$\boldsymbol{Cathode}: 2H^+ + 2e^- \rightarrow H_2 \qquad (1)$$

$$\boldsymbol{Anode}: 2H_2O \rightarrow O_2 + 4H^+ + 4e^- \qquad (2)$$

In basic conditions, the mechanism becomes:

$$\boldsymbol{Cathode}: 2H_2O + 2e^- \rightarrow 2OH^- + H_2 \quad (3)$$

$$\boldsymbol{Anode}: 4OH^- \rightarrow O_2 + 2H_2O + 4e^- \quad (4)$$

An acidic medium can be made more basic by consumption of protons in a reduction reaction, or alternatively more acidic by production of protons in an oxidation reaction (depending on the potential imposed at an electrode), and vice versa. It is important to note that the maximum pH changes occur close to the electrode and diminishes with increasing distance from the electrode.

3.1 Simulation Methods

A simulation model was designed to explore generation and diffusion of protons at the microband electrodes, using the FEA software COMSOL Multiphysics 5.3, in line with the galvanostatic model shown by Read et al. [13]. The geometry of the model consisted of a 5 mm square box as the experimental domain, and two sets of interdigitated 1 μm wide 50 nm high microband electrodes (14 protonator electrodes and 13 sensing electrodes), separated by 2 μm; see Fig. S2B and C. In the model, a flux of protons was applied to the surface of the protonators, by applying a fixed anodic current. The flux was assumed to be proportional to a galvanostatic current applied at the electrodes;

$$Flux = \frac{i}{F.A} \quad (5)$$

where “i” is the current applied, F is Faraday’s constant and A is the surface area of the electrodes. The initial pH was set to pH 7. The proton diffusion coefficient used for the simulation was 9.31 x 10^{-5} cm^2 s^{-1}. [24] Diffusion of protons was modelled according to Fick's second law. The bulk pH modelled was from pH 6 to 10. The possible effects of alkalinity, electrode separation and buffering capacity on the diffusion profiles were investigated. Interdigitated electrode array separations of 1 and 10 μm were also modelled.

The effects of a buffering agent were modelled by introduction of chemical equilibriums, as shown by Critelli et al [20] reflecting the reactions between the protons, the buffer molecule and water dissociation

$$H^+ + OH^- \rightarrow H_2O \qquad k_w = 1\,x\,10^{-14} \quad (6)$$

$$H^+ + A^- \rightarrow HA \qquad k_a = 1\,x\,10^{-6.1} \quad (7)$$

Ions, OH^-, HA and A^- were defined, reflecting the hydroxyl ion, protonated and unprotonated buffer molecules, respectively. k_w is the water dissociation constant, while k_a is the acid dissociation constant. Initial concentration of the buffer was set at 1 mM to reflect the concentration of sodium bicarbonate in the experimental buffer. The diffusion coefficients utilised: proton 9.31 x 10^{-5} cm^2 s^{-1}; hydroxyl 5.31 x 10^{-5} cm^2 s^{-1}; protonated and unprotonated buffer 1 x 10^{-5} cm^2 s^{-1} were previously reported.[20, 24]

Mesh quality is an important consideration when using FEA. As the model domain is divided into smaller sections or “elements”, the collection of lines of division are known as a mesh. A key balance to meshing is the relationship between mesh quality and its computational time or

cost. It is necessary for mesh quality to be high enough to obtain an accurate result, but a higher mesh quality results in more elements and thus a longer time to obtain a solution. Extra refinement was needed around the smaller features of the domain (the microbands) in comparison to the remainder of the domain see Fig. S2C for the meshing of domain near electrodes used in Comsol. In these experiments, a maximum error of 1% was defined. The mesh refinement was acceptable once increasing the refinement no longer produced a discernible change on the concentration profiles.

4. Results and discussion

4.1. Simulation of pH change by increasing current

FEA simulations were performed to study the generation and diffusion of protons at an interdigitated array of electrodes. A flux of protons was generated at the protonator array (surface area of 693 μm^2) by applying a galvanostatic current. Fig.1A-D show proton concentration profiles as pH values after 10 s of flux, over a range of applied currents, in a solution for which the starting pH was 7 (blue). Fig. 1A, applying a 1 nA current, presents a semicircular change in pH (colour) around the electrodes, with the largest pH change (red) closest to the electrodes. This change in colour represents the diffusion zone of the protons generated at the protonator array, with a greater pH change near the electrodes and gradually returning to bulk conditions at greater distances from the electrodes. Fig. 1B, C and D are the concentration profiles for applied currents of 10, 100 and 1000 nA, respectively, and each show a diffusion zone with an increasing diameter and a greater proportion of red (pH 4 and below) centered around the protonator electrodes for the larger currents. From equation 5 above, a larger

current generates a larger flux of protons with a resulting lower pH. Fig. 1E is a plot of solution pH in a plane 50 nm above the dielectric substrate, i.e., at the sensor electrode top surface, across the width of the domain further and illustrates that a lower pH is reached with a larger current. At each applied current, a very sharp decrease in pH observed at the center of the domain (shown in Fig. 1E at 2,500 μm on the x-axis), with a more gradual change in pH moving away from the center to the edges until bulk conditions are again observed. This enhanced drop in pH in the central regions (Fig. 1E inset) occurs directly at the electrodes since the protonators are generating protons at a higher rate than they can diffuse away thereby creating a region of lower pH above the electrodes.

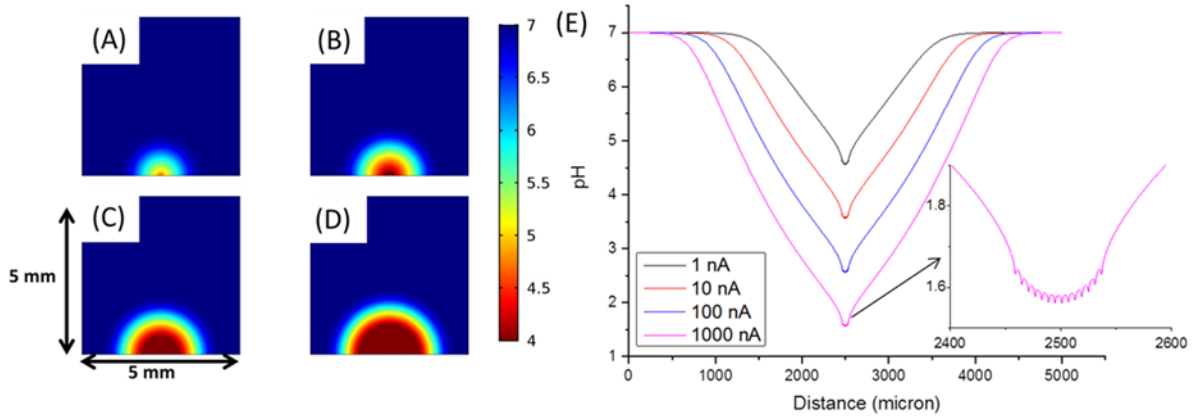

Fig. 1. The simulated pH profile after 10 s with applied current of (A) 1, (B) 10, (C) 100 and (D) 1000 nA at protonators (Surface Area 693 μm^2); (E) Plot of pH at electrode op surfaces versus width of model domain. Inset: Magnified image of region directly surrounding electrode array with an applied current of 1000 nA.

4.2. Electrode separations

Electrode separations in the interdigitated arrays of 1, 2 and 10 μm between the protonator and sensing combs were investigated after 100 μs and 1 s, respectively, for an applied current of 100 nA. It is proposed that an increasing the duration of applied current should impact the distance over which protons diffuse. We note that the 80 μm passivation window in which the array is located, a fabrication constraint, limited the number of microband electrodes that can be present as the spacing between combs increases. A 1 μm separation array contained 20 protonators and 20 sensors, a 2 μm array contains 14 protonators and 13 sensors, a 10 μm array contained 4 protonators and 4 sensors.

The Fig. 2A top panel shows the proton concentration profile after 100 μs of the 10 μm gap array. There are semicircular diffusion zones around each of the 4 protonator electrodes representing the change in pH. The clear separation between the diffusion zones is demonstrated in Fig. 2A bottom panel (black data), where bulk solution pH is still present at the sensing electrodes (the midpoint between protonators). Fig. 2A bottom panel (red data) also displays the pH after 1 second, which has been significantly decreased. After this time, the zones of decreased pH around each of the 4 protonator electrodes have overlapped significantly, though there is a small deviation of ~0.1 pH units midway between protonators (over the sensing electrodes).

Similarly, in Fig. 2B, the top panel shows the proton concentration profile after 100 μs of the 2 μm gap array. There are semicircular diffusion zones around each of the 14 protonator electrodes representing the change in pH. The overlap of these individual diffusion zones is demonstrated in Fig. 2B bottom panel (black data), where the solution pH has decreased from bulk pH at the sensing electrodes (the midpoint between protonators). Fig. 5B bottom panel (red data) shows

that the pH variation at the midpoint between protonators (i.e., at the sensors), has decreased to ~0.02 pH units after 1 s.

Finally, Fig. 2C top panel shows the proton concentration profile after 100 µs for the 1 µm gap array. There are semicircular diffusion zones around each of the 20 protonator electrodes representing the decrease in local pH. The overlap of these individual diffusion zones is demonstrated in Fig. 2C bottom panel (black data), where solution pH is now much lower at the sensing electrodes (the midpoint between protonators). With decreasing separations between the electrodes, it can be observed that the generated pH change is becoming more uniform across the array even at this short time interval. The overlap of these individual diffusion zones after 1 second is demonstrated in Fig. 2C bottom panel (red data), where the variation in pH, midpoint between protonators, is negligible. Consequently, the simulation study suggests that the pH has been sufficiently adjusted after only 1 second of pH control at these different gaps.

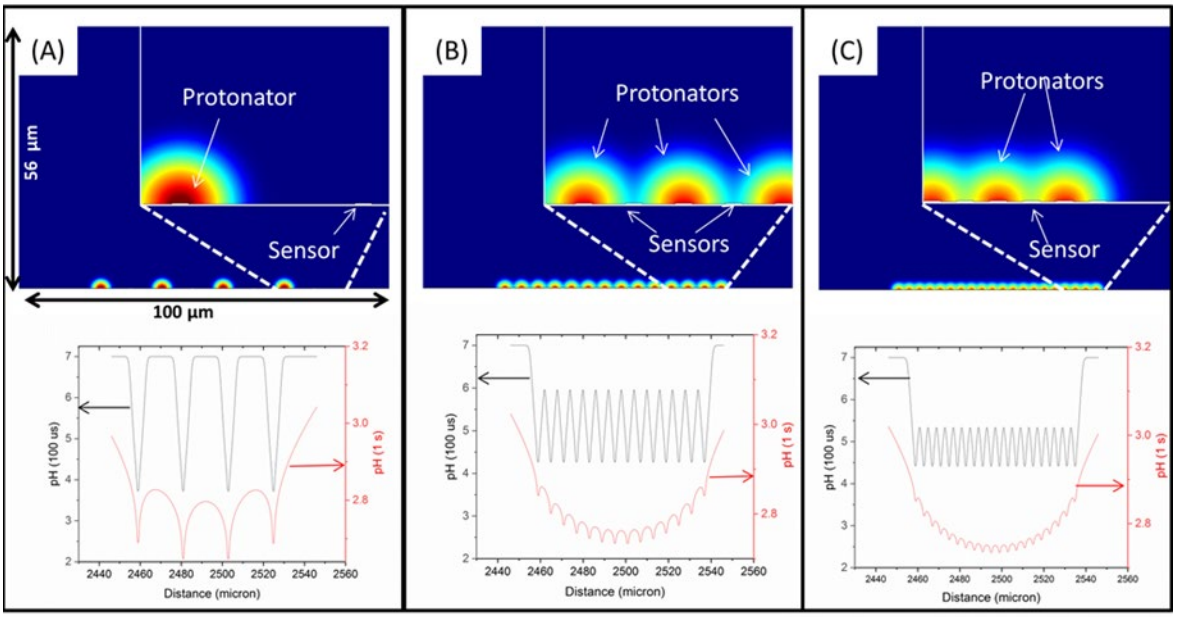

Fig. 2. Top Panel: Simulated pH profile after 100 μs with applied current of 100 nA at working electrode arrays with gaps of 10 (A), 2(B) and 1 (C) μm. Bottom Panel (A, B, C) Plots of pH at the electrodes surface for the array after 100 μs (left axis) and 1 s (right axis).

4.3. Effect of initial solution pH

The effect of varying the initial solution bulk pH, over the range of pH 6 to 10, on the final pH was investigated. To this end, only the 2 μm spacing interdigitated electrode arrays were presented as these were the electrodes utilised in the experimental study, used to confirm the model, as described below. A galvanostatic current of 100 nA was again applied to the protonators within the interdigitated electrode array. Fig. 3A shows the proton concentration profile after 100 μs of applied current with the initial bulk pH set at 6 (yellow). Individual diffusion zones observed around each of the protonators indicate the decrease in pH due to the diffusion flux of protons, highlighted by the red regions. The magnified inset shows a small degree of overlap between the diffusion zones, indicating that the local pH at the sensing electrodes remains relatively unchanged. Fig. 3B shows the equivalent simulation when the starting pH was set to 10. Again, a decrease in pH was observed following proton production at the protonators and their subsequent diffusion. The inset shows that there is relatively more overlap of the diffusion profiles and pH still appears to reach ~6.0 above the sensors. To confirm this, the final pH in the plane parallel to and 50 nm above the chip surface (i.e. at the sensor surface) is plotted in Fig. 3C where a saw tooth pH profile was observed as before across the array. The peak maxima were again located over the sensors while the peak minima were over the protonators, as expected. It was observed that regardless of the initial solution pH, a final pH of ~6.0 was achieved (pH 5.7 for starting pH 6 was reached while a final pH of 6 was reached for

starting pH 7, 9 and 10, respectively). The pH at the protonator surface was always observed to reach pH 4.2 for different starting pH values. Clearly, after 100 µs there is a change of ~1.7 pH units of the solution between the protonators and the sensors. Fig. 3D shows the equivalent simulation conditions after 1 s of applied current. Here it was observed that a final pH, with little spatial variation, of pH 2.8 was observed across the entire array. The inset shows a less magnified view to highlight the initial pH of the simulations. Consequently, these results indicate that the starting pH does not have a significant effect on achieving the final desired pH at the sensors within one second of applied protonator current. The independence from initial solution pH could allow this method of pH control to work for sensing applications in a variety of electrolytes.

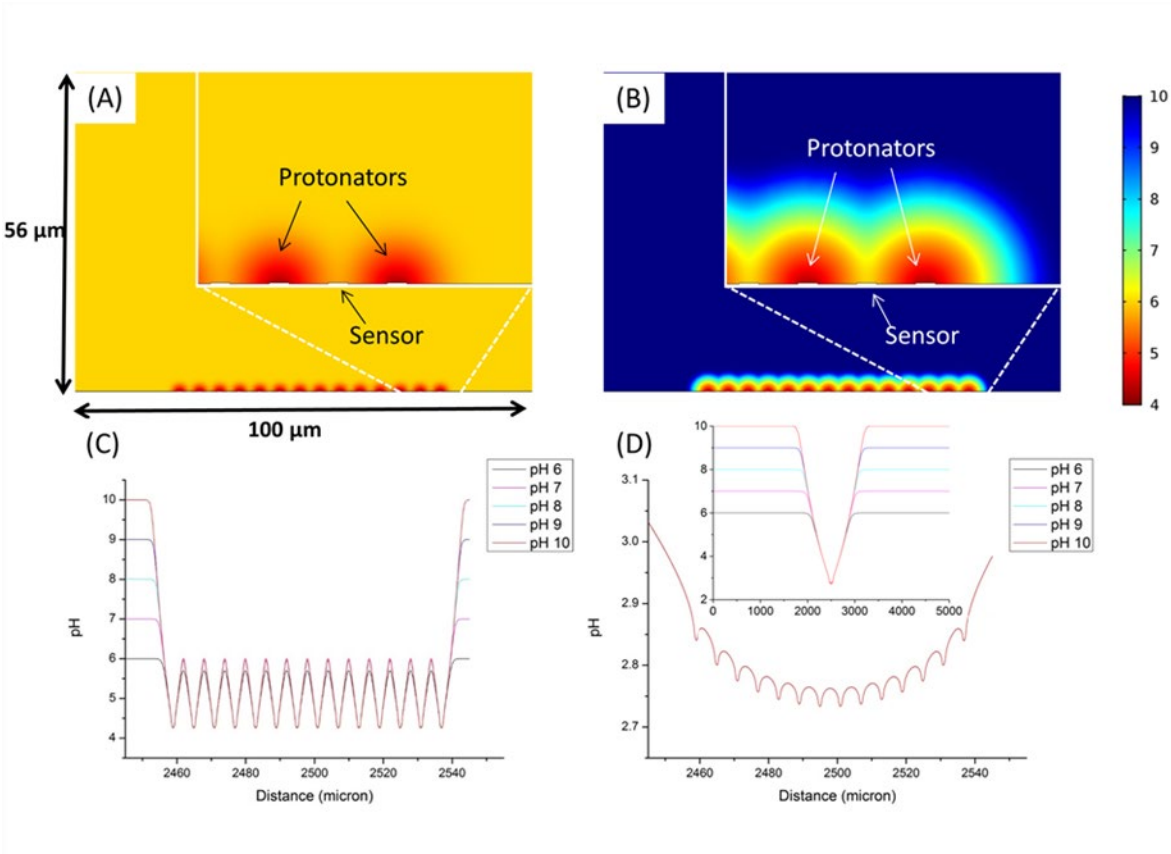

Fig. 3. Simulated pH profile after 100 μs with applied current of 100 nA at 2 μm gap working electrode arrays with starting bulk pH of 6 (A) and 10 (B). (C) and (D) show plots of the pH at the sensor electrode surface after 100 μs and 1 s respectively.

4.4. Solution buffer capacity

The model employed in the previous sections was reported by Read et al. [13] and based purely on diffusion dependence when employing a galvanostatic current. To factor in the effects of proton buffering reactions, the chemical equations (equations 5 and 6) from the Critelli et al. [20] were included to provide a more realistic model. Fig. 4 presents concentration profiles focused in on a 1 mm x 1 mm square surrounding the electrodes, which were modelled in a 5 x 5 mm boundary domain.

Simulations for an unbuffered solution are presented in Fig. S3 where the diameter of the reduced pH region was observed to be 1150 μm after 1 s and 3600 μm after 10 s, respectively. Herein, we present data for different buffer concentrations. Fig. 4A top panel is the proton concentration profile for a solution of 1 mM bicarbonate buffer after 1 s. The diameter of the region of lower pH is smaller than that of the unbuffered model (Fig. S3A). The 1 mM buffer concentration is sufficient to narrow the diameter 340 μm over which the pH change occurs, however the flux at the electrodes still reaches pH 4 and below. Fig. 4A bottom panel is the proton concentration profile for a solution with a 1 mM buffer after 10 s, where the diffusion zone diameter of tailor pH has increased to1,050 μm (but has decreased compared to 3,600 μm for unbuffered (Fig. S3B)).

The top panel of Fig. 4B is the proton concentration profile for a solution with a 10 mM buffer after 1 s. The diameter of the region of lower pH is further reduced (263 μm) and the pH at the electrodes has not reached pH 4 after 1 s. Fig. 4B bottom panel is the proton concentration profile for a solution with a 10 mM buffer after 10 s. The diffusion zone diameter has increased (740 μm) and the local pH has now decreased below pH 4. It was observed that the increased volume of protons over the additional nine second interval has surpassed the buffering capacity of the buffer.

Likewise, Fig. 4C top panel shows the proton concentration profile for a solution with a 100 mM buffer after 1 s. The colour change indicating a lower pH is barely evident (184 μm with a lowest pH of 6.57). The100 mM buffer significantly inhibits the electrochemical pH control for this applied current and duration. Fig. 4C bottom panel is the proton concentration profile for a solution with a 100 mM buffer after 10 s. Again, there is a negligible decrease in pH after the additional nine second interval; due to the buffering capacity of the 100 mM solution being greater than the flux of protons.

In Fig. 4D, the top panel is a plot of pH at the electrode surfaces after 1 second. For 1 mM buffer concentration, the pH at the protonators and sensors is as homogenous as an unbuffered solution. There is a large change in pH between the two combs for 10 mM. This buffer is effective after 1 s at scavenging protons over the 2 μm gap between the combs. Finally, there is only a slight pH difference between the combs at 100 mM. This difference being smaller than that of the 10 mM is due to the smaller relative change in pH. In the bottom panel of Fig. 4D is a plot of pH at the electrode surfaces after 10 s. Both the 1 and 10 mM buffer solutions now have the homogeneity of local pH at both electrode combs, with less of a decrease for the 10 mM buffer. For the 100 mM, buffer the same scenario exists after 10 s albeit at a slightly lower pH (6.40). These results

would suggest that to decrease the pH in high buffer concentrations would require a much higher current, which will be the subject of future work.

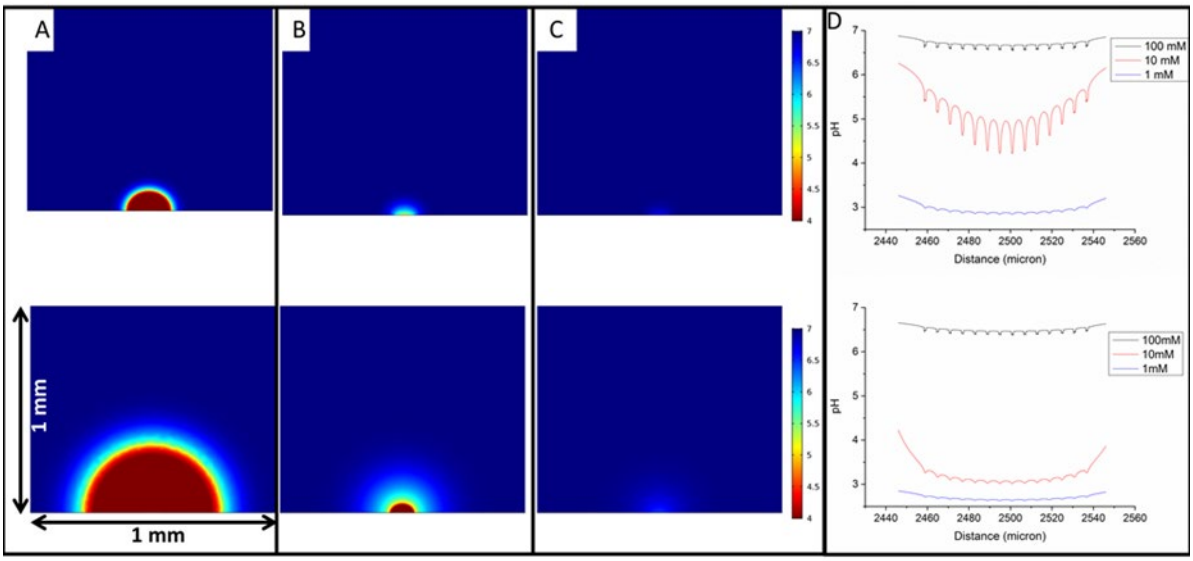

Fig. 4. Top Panel: Simulated pH profile after 1 s for an applied current of 100 nA with buffer concentration of 1 (A), 10 (B) and 100 (C) mM with (D) showing a plot of pH across the electrode surfaces; Bottom Panel: Simulated pH profile after 10 s for 100 nA with buffer concentration of 1 (A), 10 (B) and 100 (C) mM with (D) showing a plot of pH across the electrode surfaces.

4.5. Electrode characterisation

Experiments were then undertaken, using silicon chip substrates, to confirm the simulation study presented above. Interdigitated microband electrodes were fabricated as described in the experimental section. Fig. S4A shows a typical voltammogram in PBS of pH 7.4 over the potential range of -0.15 V to 1.2 V. An increase in current beginning at 0.6 V is indicative of the onset of gold oxidation during the anodic sweep. The plateau and subsequent increase at 0.75 V is indicative of the formation of a complex gold oxide morphology/ multilayers. The sharp

increase in current beginning at 1.1 V is attributed to the onset of oxygen evolution described in equations 2 and 4. On the cathodic sweep, the resultant gold oxide is then reduced at ~ -0.01 V. The electrochemical characterization was also undertaken by cyclic voltammetry of 1 mM FcCOOH from -0.15 V to 0.45 V at 100 mV/ s in both three and four electrode configurations; using the on-chip gold counter and platinum reference electrodes, respectively. Fig. S4B presents typical voltammograms obtained. In the three electrode configuration, each IDE sensing electrode array exhibited a current magnitude of ~10 nA, typical of such an array. The magnitude of this current strongly suggests that oxidation of FcCOOH only occurs at the interdigitated electrodes and that the interconnection metallization is completely passivated by the silicon nitride passivation layer. The diffusion limited peak shape arose from the electrodes of the array, i.e., not being diffusionally independent due to their close proximity, as expected[19]. By contrast, in the four electrode GC mode, a constant potential of -0.15 V was applied at the protonator electrode while the sensor electrode was scanned. A current of 28 nA was obtained at the sensing array electrodes with steady-state sigmoidal CV profiles observed. The increase in current arose from redox cycling of the FcCOOH occurring between the protonator and sensor electrodes also enabling the sensors to operate as diffusionally independent electrodes. The steady-state behavior again supports the thesis that the interconnection tracks were fully passivated and that redox reactions were only occurring at the IDEs.

4.6. Gold oxide reduction and pH control

Gold oxide was formed on the sensor electrodes by sweeping the potential positively above 1.0 V (vs. Ag/AgCl). The potential of the subsequent gold oxide reduction was used to monitor solution pH at the microband electrodes as this potential is known to be pH sensitive[4]. Fig. 5A shows an overlay of the gold oxide reduction peaks obtained at a sensor IDE immersed in

different buffer solutions prepared using different concentrations of citric acid and disodium phosphate over the pH range 3 to 8. The sensor IDE was scanned from -0.15 to 1.2 V at 100 mV/s. The reduction potential of the gold oxide was observed to increase as the pH decreased. The change in reduction potential was then plotted versus pH and presented in Fig. 5B. The plot exhibited excellent linearity with an $R^2 = 0.994$ and a super Nernstian response of -72.4 mV/pH, clearly indicating that gold oxide potential may be used as a method of pH monitoring over the timescale of these experiments (26 s). A possible reason for the super-Nernstian response is the presence of different oxidation states of gold, as shown with other metals oxide such as ruthenium and iridium when used as pH probes.[25] We note that for longer timescales, dissolution of gold from the electrode could limit this approach.

Fig. 5C shows an overlay of the gold oxide reduction peak obtained at a sensor electrode using artificial drinking water solution. The sensor IDE was again scanned from -0.15 to 1.2 V at 100 mV/s with the protonator electrode array biased at a constant potential. A variety of different potentials ranging from 1.3 to 1.70 V was applied to the protonator and the reduction potential measured. An increase in the reduction potential was observed as the applied potential is increased suggesting that the pH is decreasing as expected. This reduction peak potential was plotted against the potential applied at the protonator, presented in Fig. 5D and again exhibited very good linearity with $R^2 = 0.998$ over the timescale of the experiment. It may be concluded that these results confirm the simulation study; that the application of a suitable potential to the protonator can cause a change in solution pH (measured at the sensor electrodes), and that applying a greater potential leads to a larger change in pH, as a greater flux of protons is produced.

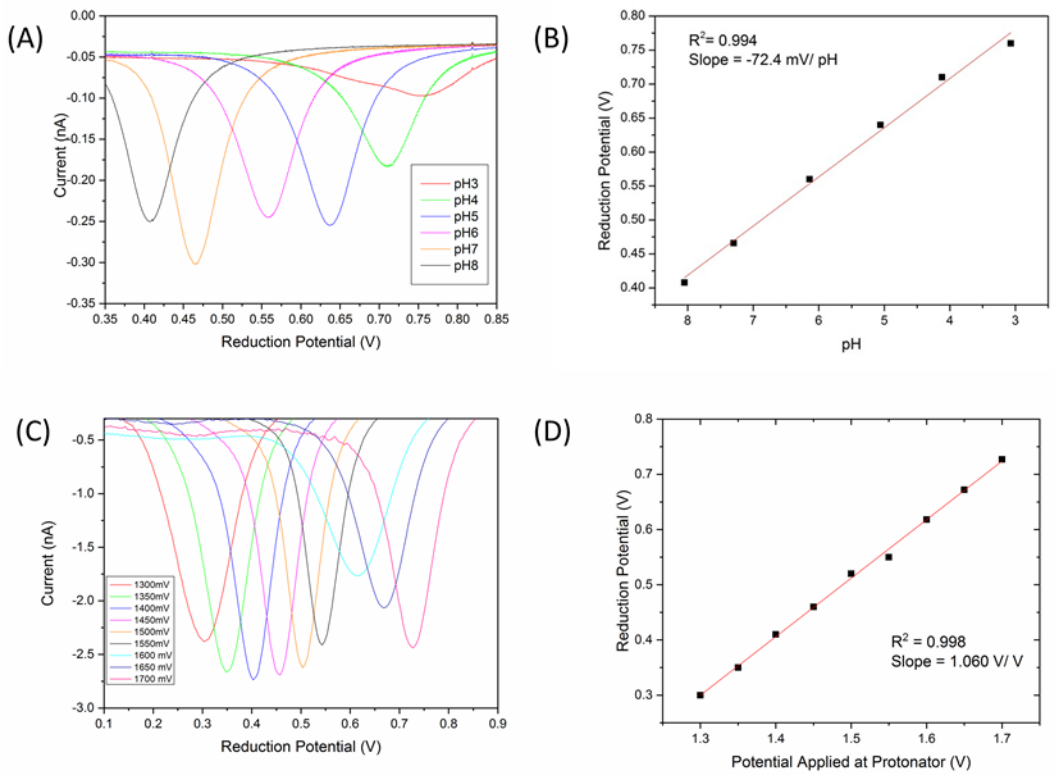

Fig. 5. Reduction peak of gold oxide in chemically controlled pH buffers (A) with calibration plot of reduction potential versus pH(B); Reduction peak of gold oxide in electrochemically pH controlled buffer (C) with calibration plot of reduction potential versus applied potential(D).

4.7. Visualization of electrochemical pH control

To further confirm the simulation study, electrochemically induced pH change was visualized experimentally by addition of 0.75 mM methyl red, a pH indicator, to a 1.5 mM solution of ADW at pH 7. Methyl red is pH sensitive and changes colour over the range of pH 4.2 (red) to 6.2 (yellow). The change of solution pH was monitored by the use of a portable potentiostat and

a microscope equipped with a CCD, as described in the experimental section. The model utilizes the diffusion coefficient of protons in water, which is then corrected for the change in viscosity due to 10% ethanol, using the Stokes-Einstein equation[26]. The simulated concentration profiles of a similarly buffered solution at pH 7 were compared to the results obtained experimentally. Fig. 6A top panel shows the simulated concentration profile at t = 0 s, while Fig. 6A bottom panel is an optical image of the electrodes t = 0. In both images, there is no change in colour as no current has been applied and consequently no change in pH has taken place. Fig. 6B top panel shows the simulated concentration profile at t = 1 s, while Fig. 6B bottom panel is the corresponding optical image of the electrodes. A colour change is visible around the electrodes in both the simulated profile and the optical image at this time. The optical colour change arises from the generated protons interacting with the methyl red in the solution, with the colour change from yellow to red indicating that the pH has decreased to pH 4.2 or below. The simulated region below pH has a diameter of ~250 μm, while the red area in the optical image has a diameter of ~215 μm, obtained using an ImageJ analysis, see Figure S5. Fig. 6C top panel shows the simulated concentration profile at t = 10 s, while Fig. 6C bottom panel is the corresponding experimental optical image of the electrodes. The diameter of the colour change has increased in both the simulated and experimental results to 750 μm and ~500 μm, respectively. Both the simulation and experiments show that the pH has changed at the sensing electrodes, the region of importance for detection of analytes.

There is a discrepancy between the total diameter of the simulation's diffusion zone and the colour change visualized experimentally. The visualization technique requires a certain colour intensity to be visible. However, it is possible that sufficient protons have diffused beyond this

visible region to ensure that the modified pH < pKa, but the colour change is not intense enough to yet be observed due to limitations of the camera and the subsequent ImageJ analysis.

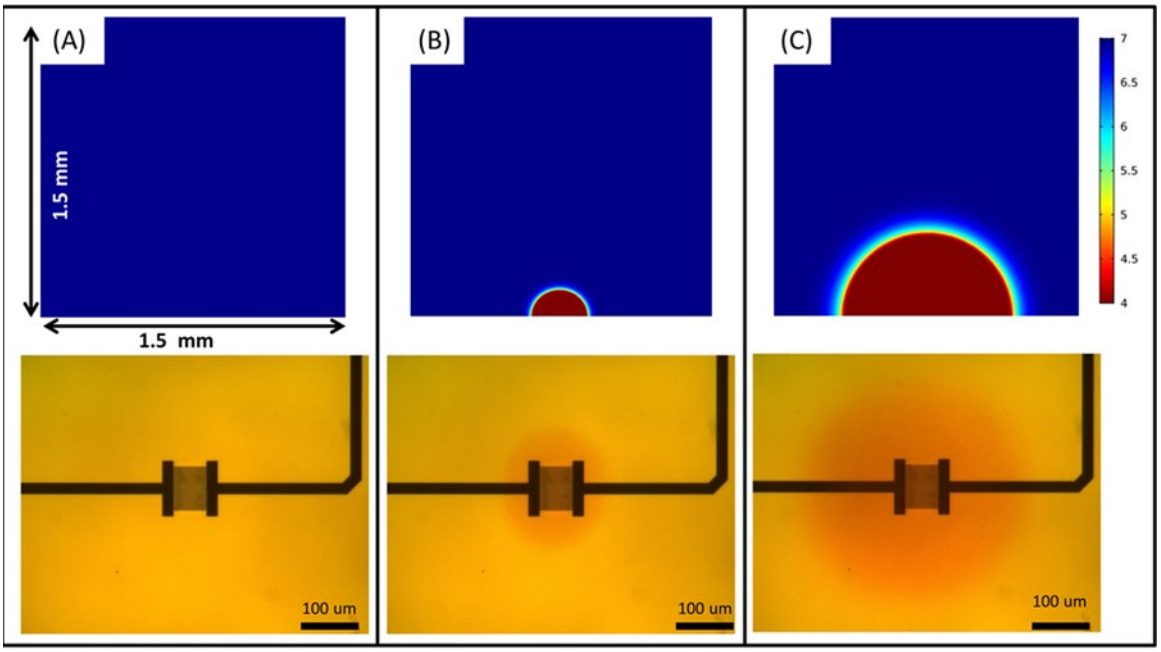

Fig. 6. Top panel: Simulated pH profile of proton generation at protonator electrodes at 0 (A), 1 (B) and 10 (C) seconds in 1 mM buffer; Bottom panel: Optical images of working electrode array as current applied at protonators at 0 (A), 1 (B) and 10 (C) seconds.

4.8. Detection of Mercury

To demonstrate pH controlled metal detection, mercury was electrodeposited from a 75 ppb (373 nM) standard solution of mercury chloride onto one comb of a gold microband electrodes by (i) using an untreated pH 7 stock solution, (ii) a solution adjusted pH of 3.5 by nitric acid addition and (iii) a pH 7 solution electrochemically modified by applying a potential of 1.74 V to the protonator comb. Figure 7 shows the corresponding stripping voltammograms from all 3

methods. As expected, the untreated pH 7 solution yielded no stripping peak, demonstrating the need to acidify the solution pH. The chemically adjusted pH method yielded an anodic stripping peak at 0.548 V with a current magnitude of 1.42 nA, while the electrochemically adjusted method yielded a stripping peat at 0.548 V with a peak magnitude of 1.45 nA (the same within experimental error). This result demonstrates that electrochemical pH control is suitable for the detection of pH dependent analytes, such as mercury.

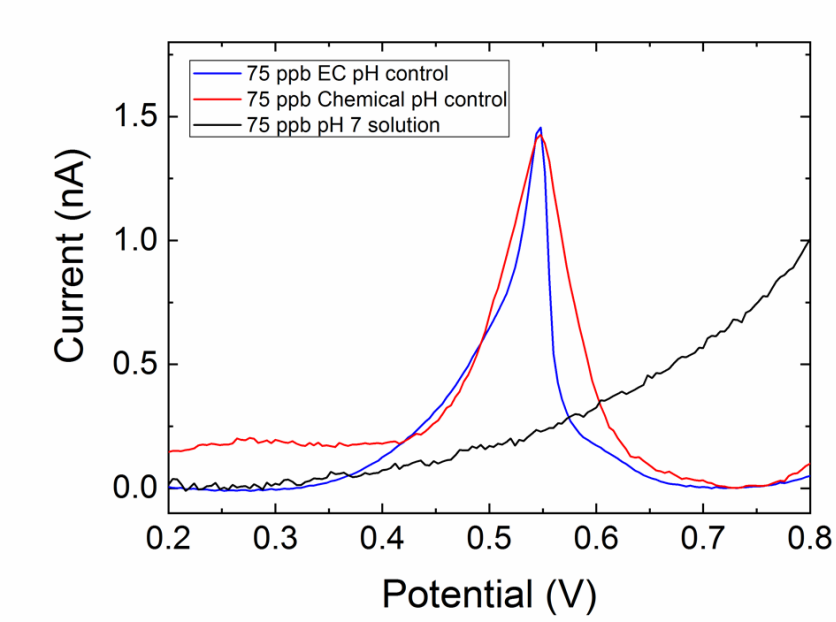

Fig. 7. SWV stripping peak of mercury in an untreated pH 7 solution, in a chemically acidified solution of pH 3.5, and a pH 7 solution with the protonator biased at 1.74 V.

5. Conclusion

We have shown a simulation and experimental study of electrochemical pH control at interdigitated gold microband arrays. The application of a galvanostatic current at the protonator

array generates protons by water electrolysis, which diffuse and reduce the local solution pH. This method allows the pH at a sensor array to be adjusted / tailored while eliminating the traditional need for the skilled handling of dangerous chemicals or the inherent expense and complexity thereof. The model has highlighted the impact of the spacing between the interdigitated electrodes, where the desired pH is reached at the sensing electrodes more rapidly at smaller distances. The initial bulk pH was shown by simulation to be largely unimportant to achieving the final desired pH at the electrode surfaces. Buffering reactions were also factored into the model, with the buffer concentration having a clear impact on the diffusion of protons from the protonator electrodes to the sensors. Microband electrodes were fabricated in line with the geometries modelled and the gold oxide reduction peak was used as a measurement proxy probe for the local solution pH at the surface of the electrodes. The pH dependent detection of mercury was performed by both chemical and electrochemical pH control. This work shows the feasibility of using a pH indicator to corroborate the region of pH change around the protonator and sensing electrodes predicted by FEA. This, in turn, supports the use of electrochemical pH control in electroanalysis, where the analytes of interest are pH dependent, such as heavy metals.

Acknowledgements

The authors would like to acknowledge funding from the Irish Research Council (Project GOIPG/2015/2925). This work has been supported in part by a research grant for the VistaMilk Centre Science Foundation Ireland (SFI); Department of Agriculture, Food and the Marine (DAFM) under Grant Number 16/RC/3835

References

[1] T.W. Kaaret, G.H. Zhang, T.C. Bruice, Electrochemistry and the dependence of potentials on pH of iron and manganese tetraphenylporphyrins in aqueous solution, Journal of the American Chemical Society, 113 (1991) 4652-4656.

[2] J. Davis, M.J. Moorcroft, S.J. Wilkins, R.G. Compton, M.F. Cardosi, Electrochemical detection of nitrate and nitrite at a copper modified electrode, The Analyst, 125 (2000) 737-742.

[3] B. Patella, R.R. Russo, A. O'Riordan, G. Aiello, C. Sunseri, R. Inguanta, Copper nanowire array as highly selective electrochemical sensor of nitrate ions in water, Talanta, 221 (2021) 121643.

[4] I. Seymour, B. O'Sullivan, P. Lovera, J.F. Rohan, A. O'Riordan, Electrochemical detection of free-chlorine in Water samples facilitated by in-situ pH control using interdigitated microelectrodes, Sensors and Actuators B: Chemical, 325 (2020) 128774.

[5] L.A. Wasiewska, I. Seymour, B. Patella, R. Inguanta, C.M. Burgess, G. Duffy, A. O'Riordan, Reagent free electrochemical-based detection of silver ions at interdigitated microelectrodes using in-situ pH control, Sensors and Actuators B: Chemical, 333 (2021) 129531.

[6] R.J. Toh, W.K. Peng, J. Han, M. Pumera, Haemoglobin electrochemical detection on various reduced graphene surfaces: well-defined glassy carbon electrode outperforms the graphenoids, RSC Advances, 4 (2014) 8050-8054.

[7] A. Ganguly, P. Rice, K.C. Lin, S. Muthukumar, S. Prasad, A Combinatorial Electrochemical Biosensor for Sweat Biomarker Benchmarking, SLAS Technol, 25 (2020) 25-32.

[8] B. Patella, A. Sortino, G. Aiello, C. Sunseri, R. Inguanta, Reduced graphene oxide decorated with metals nanoparticles electrode as electrochemical sensor for dopamine, 2019 IEEE International Conference on Flexible and Printable Sensors and Systems (FLEPS), 2019, pp. 1-3.

[9] G.A.S. Minero, P.F. Wagler, A.A. Oughli, J.S. McCaskill, Electronic pH switching of DNA triplex reactions, RSC Advances, 5 (2015) 27313-27325.

[10] P.A. Michaud, M. Panizza, L. Ouattara, T. Diaco, G. Foti, C. Comninellis, Electrochemical oxidation of water on synthetic boron-doped diamond thin film anodes, Journal of Applied Electrochemistry, 33 (2003) 151-154.

[11] B. Kumar Jena, C. Retna Raj, Gold Nanoelectrode Ensembles for the Simultaneous Electrochemical Detection of Ultratrace Arsenic, Mercury, and Copper, Analytical Chemistry, 80 (2008) 4836-4844.

[12] P. Salaün, C.M.G. van den Berg, Voltammetric Detection of Mercury and Copper in Seawater Using a Gold Microwire Electrode, Analytical Chemistry, 78 (2006) 5052-5060.

[13] T.L. Read, E. Bitziou, M.B. Joseph, J.V. Macpherson, In Situ Control of Local pH Using a Boron Doped Diamond Ring Disk Electrode: Optimizing Heavy Metal (Mercury) Detection, Analytical Chemistry, 86 (2014) 367-371.

[14] B. Patella, S. Piazza, C. Sunseri, R. Inguanta, NiO Thin Film for Mercury Detection in Water by Square Wave Anodic Stripping Voltammetry, 2017.

[15] A. Wahl, K. Dawson, J. MacHale, S. Barry, A.J. Quinn, A. O'Riordan, Gold nanowire electrodes in array: simulation study and experiments, Faraday Discussions, 164 (2013) 377-390.

[16] N. Godino, X. Borrisé, F.X. Muñoz, F.J. del Campo, R.G. Compton, Mass Transport to Nanoelectrode Arrays and Limitations of the Diffusion Domain Approach: Theory and Experiment, The Journal of Physical Chemistry C, 113 (2009) 11119-11125.

[17] D.W.M. Arrigan, G. Herzog, Theory of electrochemistry at miniaturised interfaces between two immiscible electrolyte solutions, Current Opinion in Electrochemistry, 1 (2017) 66-72.

[18] M. Yang, R.G. Compton, Adsorption processes coupled with mass transport at macro-electrodes: New insights from simulation, Journal of Electroanalytical Chemistry, 836 (2019) 68-76.

[19] A.J.C. Wahl, I.P. Seymour, M. Moore, P. Lovera, A. O'Riordan, J.F. Rohan, Diffusion profile simulations and enhanced iron sensing in generator-collector mode at interdigitated nanowire electrode arrays, Electrochimica Acta, 277 (2018) 235-243.

[20] R.A.J. Critelli, M. Bertotti, R.M. Torresi, Probe effects on concentration profiles in the diffusion layer: Computational modeling and near-surface pH measurements using microelectrodes, Electrochimica Acta, 292 (2018) 511-521.

[21] A. Montrose, N. Creedon, R. Sayers, S. Barry, A. O'Riordan, Novel Single Gold Nanowire-based Electrochemical Immunosensor for Rapid Detection of Bovine Viral Diarrhoea Antibodies in Serum, Journal of Biosensors & Bioelectronics, 6 (2015).

[22] T.L. Read, M.B. Joseph, J.V. Macpherson, Manipulation and measurement of pH sensitive metal–ligand binding using electrochemical proton generation and metal detection, Chemical Communications, 52 (2016) 1863-1866.

[23] J. Rossmeisl, A. Logadottir, J.K. Nørskov, Electrolysis of water on (oxidized) metal surfaces, Chemical Physics, 319 (2005) 178-184.

[24] S.H. Lee, J.C. Rasaiah, Proton transfer and the mobilities of the H+ and OH− ions from studies of a dissociating model for water, The Journal of Chemical Physics, 135 (2011) 124505.

[25] K. Singh, B.-S. Lou, J.-L. Her, S.-T. Pang, T.-M. Pan, Super Nernstian pH response and enzyme-free detection of glucose using sol-gel derived RuOx on PET flexible-based extended-gate field-effect transistor, Sensors and Actuators B: Chemical, 298 (2019) 126837.

[26] S. Song, C. Peng, Viscosities of Binary and Ternary Mixtures of Water, Alcohol, Acetone, and Hexane, Journal of Dispersion Science and Technology, 29 (2008) 1367-1372.